CrossMark

n-Butyl Acetate Synthesis in the Presence of Pyridinium-Based Acidic Ionic Liquids: Influence of the Anion Nature

Ivaylo Tankov[1] · Magdalena Mitkova[1] · Radoslava Nikolova[1] · Anife Veli[1] ·
Dicho Stratiev[2]

Abstract The catalytic behavior of three Brønsted acidic ionic liquids: pyridinium hydrogen sulfate ([H–Pyr]$^+$[HSO$_4$]$^-$), pyridinium dihydrogen phosphate ([H–Pyr]$^+$[H$_2$PO$_4$]$^-$) and pyridinium nitrate ([H–Pyr]$^+$[NO$_3$]$^-$) in the esterification of acetic acid with *n*-butanol was compared in the current paper. The alteration in the values of acetic acid conversion and esterification rate were investigated as a function of the process parameters: catalyst nature, catalyst loading, initial molar ratio *n*-butanol:acetic acid and reaction temperature. The anion variety modified the acidity of the obtained samples and effected their catalytic activity as follows: [H–Pyr]$^+$[NO$_3$]$^-$ < [H–Pyr]$^+$[H$_2$PO$_4$]$^-$ < [H–Pyr]$^+$[HSO$_4$]$^-$. The increasing of both catalyst loading and reaction temperature led to higher values of acetic acid conversion and esterification rate. The existence of a positive linear relationship between the esterification rate and acetic acid concentration was observed. The increasing of the *n*-butanol concentration negatively affected the rate of esterification. The acetic acid conversion was improved as the initial molar ratio *n*-butanol-to-acetic acid was raised.

Graphical Abstract
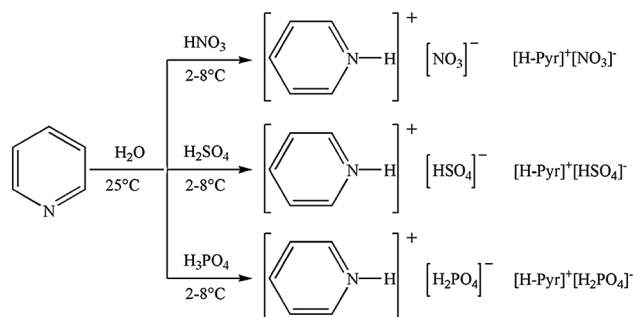
1 Introduction

Esterification of carboxylic acids is an important reaction in chemical and pharmaceutical industries [1]. The simplest route to produce esters with high yield is the direct esterification of acids with alcohol in the presence of homogeneous or heterogeneous catalyst.

Esterification is a very slow and highly reversible reaction. Consequently, the conversion of the reactants is determined by the equilibrium [2–4]. Since, the equilibrium constant of esterification reaction is in the range of 1–10, considerable amounts of reactants exit in the equilibrium mixture. Being a reversible reaction, the reagent conversion during esterification can be generally improved by the following methods: (1) using alcohol in large excess and (2) removal of water by physical means such as distillation. Taking into account that the limiting step in the esterification reaction is the protonation (activation) of carboxylic

✉ Ivaylo Tankov
   igtankov@yahoo.com

[1] University "Prof. Dr. Assen Zlatarov" Burgas, Burgas 8010, Bulgaria

[2] LUKOIL Neftohim Burgas, Burgas 8010, Bulgaria

⌂ Springer

acid, both homogeneous and heterogeneous acids can accelerate the reaction.

The conventional industrial esterification of acetic acid with *n*-butanol for production of *n*-butyl acetate (Fig. 1) is carried out in batch process using mineral acids (sulphuric, hydrofluoric, phosphoric) as catalysts [5]. However, this process leads to some serious problems such as side reactions (mainly dehydration of *n*-butanol to dibutyl ether), corrosion of equipment and hard isolation of product. To overcome these drawbacks, solid heterogeneous catalysts such as heteropoly acids [6], molecular sieves [7], resins [1, 8, 9] and supported metal oxides [10, 11] are extensively studied.

Brønsted acidic ionic liquids (BAILs), compounds which possess negligible volatility, excellent thermal stability, remarkable solubility and structural variety [7–9], are thought to be promising catalysts for esterification of acetic acid with various alcohols [12–17]. For example, Bourahla et al. [12] investigated the catalytic performance of BAILs, containing hydrogen sulphate anion ([HSO$_4$]$^-$) and different cation (l-butyl-3-methylimidazolium hydrogen sulphate, l-hexyl-3-methylimidazolium, l-butyl-3-methylimidazolium dihydrogen phosphate and l-[2-(2-hydroxyethoxy)-ethyl]-3-methylimidazolium hydrogen sulphate) in esterification of acetic acid with C$_5$–C$_7$ and C$_{10}$ alcohols. Similar to Bourahla et al. [12], Tao at al [13]. presented the esterification of acetic acid with C$_1$–C$_4$ alcohols in the presence of 1-methylimidazole hydrogen sulfate, N-triethylammonium hydrogen sulfate, butyl triethylammonium hydrogen sulfate and N-(4-sulfonic acid) butyl triethylammonium sulfate. Authors reported that the esterification process depends mainly on both the acidity and hydrophilic nature of the catalysts.

The effect of cation variety on the catalytic behavior was also determined by Zhao et al. [15] for esterification of acetic acid with 1-pentanol in the presence of 3-methyl-1-imidazole)-ethylene hydrogen sulphate, 3-methyl-1-imidazole)-propylene hydrogen sulphate and 3-methyl-1-imidazole)-butylene hydrogen sulphate.

It was generally accepted that higher acidity of the anion in the ionic liquid results in higher yield of the ester [13, 18, 19]. In the light of this, Duan et al. [14] showed that the esterification of acetic acid with cyclic olefins, catalyzed by ionic liquid (2-methylpyridinium trifluoroacetate, 2-methylpyridinium trifluoromethanesulfonate, 2-methylpyridinium methanesulfonate) proceeds with high selectivity and product yield. In addition, the kinetics of *n*-butyl acetate

synthesis in the presence of ionic liquids with different cations ([N$_{2224}$]$^+$, [BSEt$_3$N]$^+$, [H–Pyr]$^+$, [Et$_3$N–H]$^+$ and [H–Mim]$^+$) was extensively studied by Tao et al. [2]. However, the published studies focused on different anion nature for promoting of acetic acid esterification with *n*-butanol are limited. Hence, the investigation of the catalytic activity of ionic liquids with variety of the anion seems to be necessary. On the other hand, the industrial application of a process requires the usage of an inexpensive catalyst that can be easily regenerated. Therefore, the current paper reported the synthesis of low-cost ionic liquids containing traditional cation [H–Pyr]$^+$ and different anions ([H$_2$PO$_4$]$^-$, [HSO$_4$]$^-$ and [NO$_3$]$^-$) for esterification of acetic acid with *n*-butanol. Infrared spectroscopy and thermogravimetric analysis were used as characterization methods. In addition, the influence of the process parameters on the acetic acid conversion and esterification rate was also discussed.

2 Experimental

2.1 Chemicals

Acetic acid (99.95 wt%), *n*-butanol (99 wt%), pyridine (99 wt%), sulphuric acid (98 wt%), phosphoric acid (85 wt%) and nitric acid (65 wt%) are purchased from Merck. Diethyl ether is obtained from Sigma-Aldrich, while hexane (99.4 wt%) and heptane (99.8 wt%) are supplied by Riedel-de Haën. All chemicals are used without any further purification.

2.2 Catalysts Preparation

The current article presents the synthesis of three ionic liquids, composed of [H–Pyr]$^+$cation and different anions ([NO$_3$]$^-$, [HSO$_4$]$^-$ and [H$_2$PO$_4$]$^-$) (Fig. 2). Preparation procedure of the acidic ionic liquid [H–Pyr]$^+$[NO$_3$]$^-$, [H–Pyr]$^+$[HSO$_4$]$^-$ and [H–Pyr]$^+$[H$_2$PO$_4$]$^-$ is similar to those described by Tao et al. [13] and Duan et al. [14].

Pyridine (51.06 g, 0.6455 mol) and ultra clean water (34.86 g, 1.9365 mol) were charged into a 0.250 L three-necked flat bottom reactor, equipped with a magnetic stirring, reflux condenser and thermometer. The aqueous solution of pyridine (C$_{pyr}$=7.4195 mol/L) was stirred at ambient temperature for 30 min, where after the temperature was reduced up to 2–8 °C. Then nitric acid (40.67 g, 0.6455 mol) was added dropwise over a period of 90 min

Fig. 1 Esterification of acetic acid with *n*-butanol in the presence of acidic catalyst
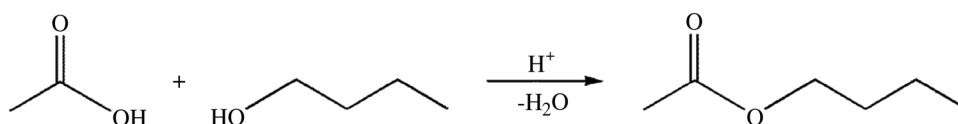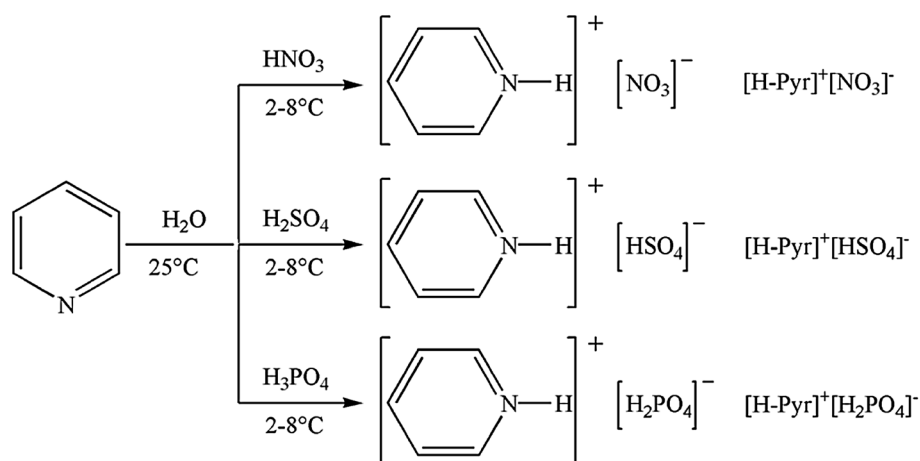
Fig. 2 Synthesis of pyridinium-based ionic liquids

under vigorous stirring. The reaction mixture was stirred at reflux for an additional period of 5 h at 80 °C.

For solvent removing, the aqueous solution of pyridinium nitrate was distilled at 60 °C and reduced pressure (0.050 MPa) and the product was dried under the same conditions for 8 h until the weight of the residue remained constant. After cooling, the resulting white-colored solid ([H–Pyr]$^+$[NO$_3$]$^-$) was washed with diethyl ether 0.100 L for three times and dried in vacuum (0.050 MPa) at 80 °C for 12 h. Preparation protocol of the ionic liquids [H–Pyr]$^+$[HSO$_4$]$^-$ and [H–Pyr]$^+$[H$_2$PO$_4$]$^-$ did not differ from that of [H–Pyr]$^+$[NO$_3$]$^-$.

2.3 Infrared Spectroscopy

Infrared spectra of pure pyridine, [H–Pyr]$^+$[NO$_3$]$^-$, [H–Pyr]$^+$[HSO$_4$]$^-$ and [H–Pyr]$^+$[H$_2$PO$_4$]$^-$ samples were recorded using Nicolet iS 50 Thermo Scientific FT-IR spectrophotometer in the frequency region of 4000–400 cm^{-1}. Infrared spectra of pure pyridine and [H–Pyr]$^+$[HSO$_4$]$^-$ were measured by means of KBr pellets, while those of [H–Pyr]$^+$[NO$_3$]$^-$ and [H–Pyr]$^+$[H$_2$PO$_4$]$^-$ using Nujol.

2.4 Thermal Gravimetric Analysis

Thermal stability of [H–Pyr]$^+$[NO$_3$]$^-$, [H–Pyr]$^+$[HSO$_4$]$^-$ and [H–Pyr]$^+$[H$_2$PO$_4$]$^-$ ionic liquids was investigated in NETZSCH STA 449 F3 instrument. The samples are heated from 25 to 700 °C at 10 °C/min under stream of nitrogen (0.020 L min).

2.5 Apparatus

The experiments were carried out in a three-necked round bottom flask of 0.250 L capacity, equipped with condenser, Dean–Stark trap, a port for sample withdrawal and thermometer. Mixing of the reaction fluid was performed by a magnetic stirrer.

2.6 Catalytic Test

A typical procedure for the esterification of acetic acid with *n*-butanol (Fig. 2) was as follows. Acetic acid (0.2778 mol) and ionic liquid (5, 10 or 15 wt% with respect to the mass of acetic acid) were placed in the reactor. Hexane (0.2778 mol) or heptane (0.2778 mol) was added to the reaction mixture for water removal in the form of azeotrope mixture during the reaction progress. Once the desired reaction temperature (80 and 100 °C) was attained, a known quantity of *n*-butanol (0.2778, 0.8834, 1.3890 and 1.9446 mol to reach an *n*-butanol-to-acetic acid molar ratio (N_B/N_A) of 1/1, 3/1, 5/1 and 7/1, respectively), separately heated to the set temperature was added into the reactor. This time was considered as the zero reaction time (t = 0).

The samples (1 ml) were withdrawn at regular intervals of time (20 min) and immediately cooled in an ice bath. The acetic acid concentration was analyzed using GC 7890A (Agilent Technologies), equipped with a flame ionization detector (FID) and capillary column HP-INNO-WAX, 30 m × 0.32 mm × 0.25 μm. High purity helium was used as a carrier gas at a flow rate of 0.0015 L min. The oven temperature was programmed at 70 °C for 2 min and then it was raised from an initial value of 70–160 °C at a ramp rate of 5 °C/min. The injector and detector temperature were maintained at 250 and 300 °C, respectively. The acetic acid conversion was calculated according to Eq. 1:

$$X_A = \left(C_{A0} - C_A\right)/C_{Ao} \tag{1}$$

where X_A is the acetic acid conversion (%); C_{A_0} is the initial acetic acid concentration (mol/L) and C_A corresponds to the acetic acid concentration (mol/L) at reaction time t (min).

2.7 Kinetic Model

In this work, the esterification of acetic acid with n-butanol in the presence of $[H–Pyr]^+[HSO_4]^-$, $[H–Pyr]^+[H_2PO_4]^-$ and $[H–Pyr]^+[NO_3]^-$ catalysts was proposed as a second-order reversible reaction. Based on this, a pseudo-homogeneous kinetic model was presented (Eq. (2)).

$$-r_A = -\frac{dC_A}{dt} = k_1 C_A C_Y - k_2 C_B C_Z \qquad (2)$$

where C_A, C_Y, C_B and C_Z describe the concentration (mol/L) of acetic acid, n-butanol, ester and water at reaction time t (min), respectively.

Assuming that the reaction products (B and Z) do not present in the initial reaction mixture and the esterification reaction is conducted via reactive distillation process (expressed by continuous removal of water in the form of azeotrope), Eq. (2) becomes as follows:

$$\frac{1}{C_{A0}(M-1)}\left(\ln \frac{M - X_A}{M(1 - X_A)}\right) = k_1 t \qquad (3)$$

where M denotes the initial reactants molar ratio. The left hand side of the Eq. (3) has dimension L/mol. The plot of $\frac{1}{C_{A0}(M-1)}\left(\ln \frac{M-X_A}{M(1-X_A)}\right)$ versus time (t) is a straight line passing through origin. The slope of the line represents the kinetic constant (k) value with dimension L/mol.min.

3 Results and Discussion

3.1 Infrared Spectroscopy

Infrared spectra of the obtained ionic liquids $[H–Pyr]^+[HSO_4]^-$, $[H–Pyr]^+[H_2PO_4]^-$ and $[H–Pyr]^+[NO_3]^-$ in frequency region of 2000–400 cm^{-1} are shown in Fig. 3. For comparison, the infrared spectrum of pure pyridine was also included.

It was observed that the infrared spectrum of pure pyridine contains characteristic bands at 607, 702, 749, 993, 1028, 1070, 1147, 1217, 1437, 1483 and 1579 cm^{-1} (Fig. 3). The peaks at 607, 707 and 1028 cm^{-1} are due to bending vibrations in aromatic ring, while those at 749, 993, 1070, 1147 and 1217 cm^{-1} represent the wagging vibrations of C–H bonds in –CH$_2$ groups [20]. The characteristic bands 1437, 1483 and 1579 cm^{-1} denote a variety in C=C and C=N bonds length in aromatic core.

Results showed that the interaction between pyridine and sulphuric acid (synthesis of ionic liquid $[H–Pyr]^+[HSO_4]^-$) leads to a significant alteration in the infrared spectrum of pyre pyridine (Fig. 3). The latter was confirmed by a disappearance of the characteristic bands at 1437 and 1579 cm^{-1} in infrared spectrum of pyre pyridine and developing of new ones at 576, 883, 1001, 1064, 1173, 1546 and 1639 cm^{-1} in infrared spectrum of $[H–Pyr]^+[HSO_4]^-$. The intensive peaks at 576 and 1173 cm^{-1}, and the bands at 1001 and 1064 cm^{-1} characterize bond vibrations in hydrogen sulphate anion ($[HSO_4]^-$). The first two peaks are due to symmetrical vibrations of S=O bond, while the latter two ones denote S–OH stretches [21, 22].
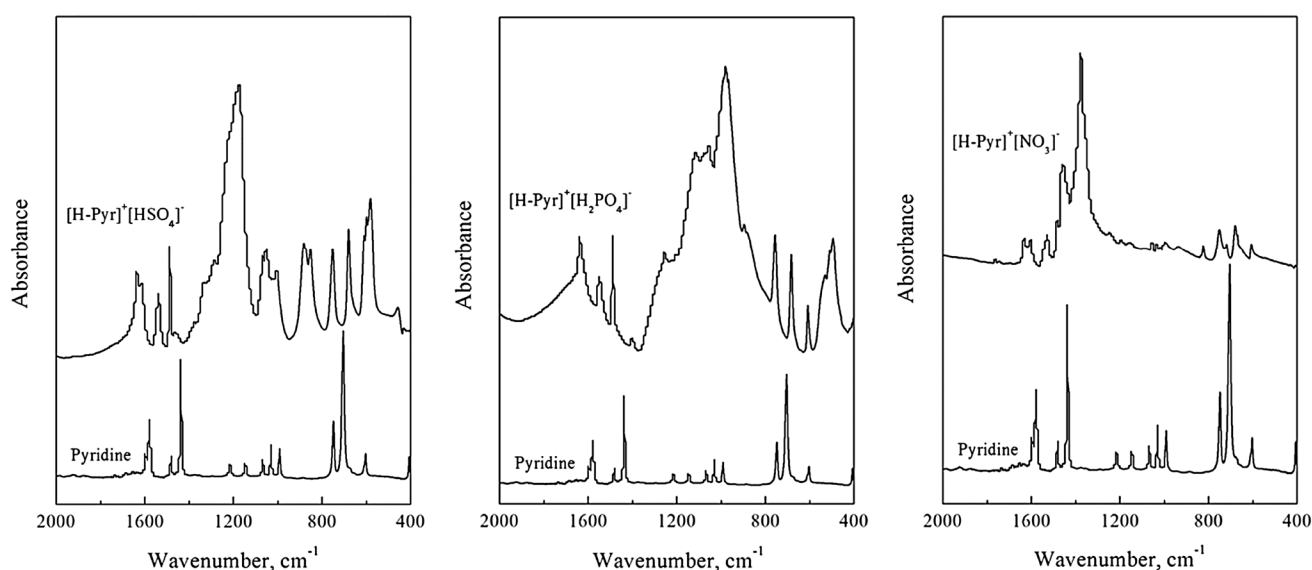

Fig. 3 Infrared spectra of pure pyridine and the ionic liquids $[H–Pyr]^+[HSO_4]^-$, $[H–Pyr]+[H_2PO_4]^-$ and $[H–Pyr]^+[NO_3]^-$

The characteristic bands at 1546 and 1639 cm^{-1} in infrared spectrum of [H–Pyr]$^+$[HSO$_4$]$^-$ illustrate a vibration of N–H bond in [H–Pyr]$^+$ cation [23, 24]. In other words, the bands at 1546 and 1639 cm^{-1} indicate the formation of pyridinium cation.

Figure 3 presents the infrared spectrum of [H–Pyr]$^+$[H$_2$PO$_4$]$^-$ sample. It contains bands at 492, 534, 889 (shoulder), 979, 1054, 1110, 1250, 1530 and 1636 cm^{-1}. The bands at 492, 534, 1054 and 1110 cm^{-1} characterize the O=P=O group in anion [H$_2$PO$_4$]$^-$. In details, the peak at 492 cm^{-1} was associated with out-of-plane bending vibration, while those at 492, 534, 1054 and 1110 cm^{-1} were due to rocking, symmetric and asymmetric vibration, respectively [25]. The out-of-plane and in-plane P–OH deformation vibrations were registered by the appearance of a shoulder and a peak at 889 and 1250 cm^{-1}, respectively. The band at 979 cm^{-1} shows a stretching vibration of HO–P–OH atomic group [26]. The vibration of N–H bond in pyridinium cation ([H–Pyr]$^+$) is presented by peaks at 1530 and 1636 cm^{-1}.

The infrared spectrum of [H–Pyr]$^+$[NO$_3$]$^-$ illustrates the appearance of peaks at 672, 826, 1055, 1376 and 1758 cm^{-1} (Fig. 3). The peaks of low intensity at 672, 826 and 1758 cm^{-1} are attributed to vibrational stretching of O=N–O$^-$ group, while the prominent band at 1376 cm^{-1} characterizes an asymmetric valence vibration in nitrate anion ([NO$_3$]$^-$).

Batsanov [27] investigated the crystal structure of pyridinium nitrate at 25 °C and showed the existence of a strong hydrogen bond between the pyridinium cation ([H–Pyr]$^+$) and nitrate anion (Fig. 4). The latter was detected by the presence of a peak at 1055 cm^{-1} in infrared spectrum of [H–Pyr]$^+$[NO$_3$]$^-$ (Fig. 3) [28]. Similar to [H–Pyr]$^+$[H$_2$PO$_4$]$^-$ sample, infrared spectrum of ionic liquid [H–Pyr]$^+$[NO$_3$]$^-$ also contains bands (at 1530 and 1636 cm^{-1}) due to N–H bond vibration in pyridinium cation.

3.2 Thermogravimetric Analysis

TGA curves of ionic liquids [H–Pyr]$^+$[HSO$_4$]$^-$, [H–Pyr]$^+$[H$_2$PO$_4$]$^-$ and [H–Pyr]$^+$[NO$_3$]$^-$ are shown in Fig. 5. The thermal behavior of [H–Pyr]$^+$[HSO$_4$]$^-$ sample
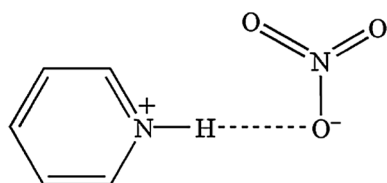
Fig. 4 Formation of hydrogen bond between pyridinium cation ([H–Pyr]$^+$) and nitrate anion ([NO$_3$]$^-$) in ionic liquid [H–Pyr]$^+$[NO$_3$]$^-$
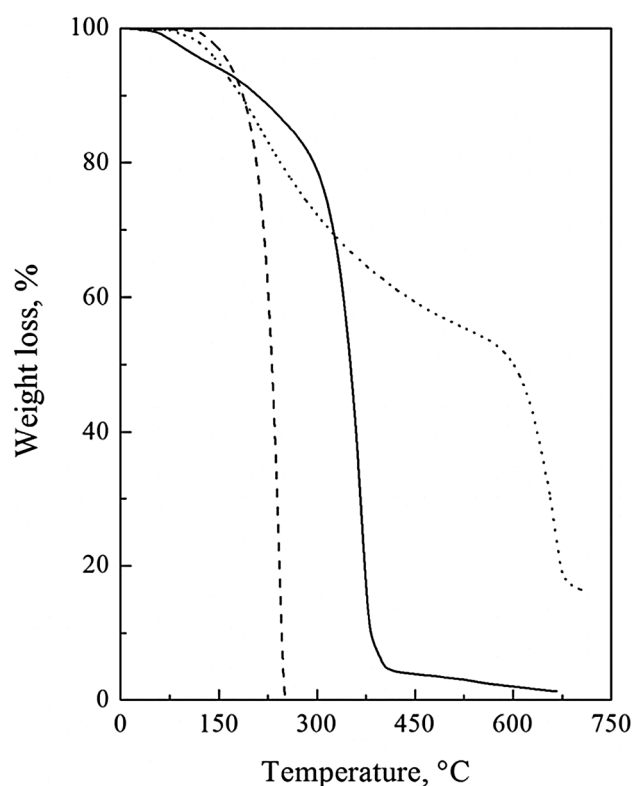
Fig. 5 TGA curves and weight loss of [H–Pyr]$^+$[HSO$_4$]$^-$ (*solid line*), [H–Pyr]$^+$[H$_2$PO$_4$]$^-$ (*dot line*) and [H–Pyr]$^+$[NO$_3$]$^-$ (*dash line*)

measured by TG includes three main regions of weight loss: (*i*) from room temperature to 125 °C, (*ii*) from 167 to 256 °C and (*iii*) between 273 and 397 °C. The weight loss (3.47%) in the first temperature region can be assigned to the elimination of physically adsorbed water, while the second step of weight loss (6.50%) was correlated with the removal of crystalline water. The weight loss (85.02%) determined in the last region was connected with molecular destruction of the sample [13].

Thermogravimetric analysis showed that [H–Pyr]$^+$[H$_2$PO$_4$]$^-$ possesses higher thermal stability compared to that of [H–Pyr]$^+$[HSO$_4$]$^-$. Two temperature areas of weight loss were detected: a wide one from 129 to 528 °C and a sharp one from 588 to 701 °C. In the first temperature region the weight of sample decreases with 41.53% due to elimination of physically adsorbed water and partial decomposition processes. The sharp temperature region (588–701 °C) showed that the mass of sample decreases up to 19.32% due to thermal destruction. Consequently, the complete thermal decomposition of ionic liquid [H–Pyr]$^+$[H$_2$PO$_4$]$^-$ occurs at temperatures higher than 700 °C. Figure 5 clearly indicates that among all samples, [H–Pyr]$^+$[NO$_3$]$^-$ possesses the lowest thermal stability. Derivatogram of [H–Pyr]$^+$[NO$_3$]$^-$ contains a sharp region of weight loss between 122 and 251 °C,

where complete thermal decomposition of the sample was observed.

It can be summarized that the ionic liquids $[H–Pyr]^+[HSO_4]^-$, $[H–Pyr]^+[H_2PO_4]^-$ and $[H–Pyr]^+[NO_3]^-$ usage as catalysts for esterification catalysts requires temperatures lower than 120 °C.

3.3 Catalytic Activity

The catalytic activity of $[H–Pyr]^+[NO_3]^-$, $[H–Pyr]^+[H_2PO_4]^-$ and $[H–Pyr]^+[HSO_4]^-$ samples was evaluated by the variation of acetic acid conversion (X_A) during esterification with *n*-butanol (Fig. 6). For comparison, the value of acetic acid conversion for non-catalyzed (blank) reaction was also included.

It is well known that a crucial step in the esterification of carboxylic acids is the formation of active carbonyl complex (pronated acid) as a result of carboxylic acid–catalyst interaction [29, 30]. The number of those active complexes is directly proportional to the extent of catalyst acidity. In other words, the concentration of pronated acid is correlated to the catalyst capacity (expressed by acid dissociation constant K_A) to produce hydrogen cations (protons, H^+) [2, 31, 32].
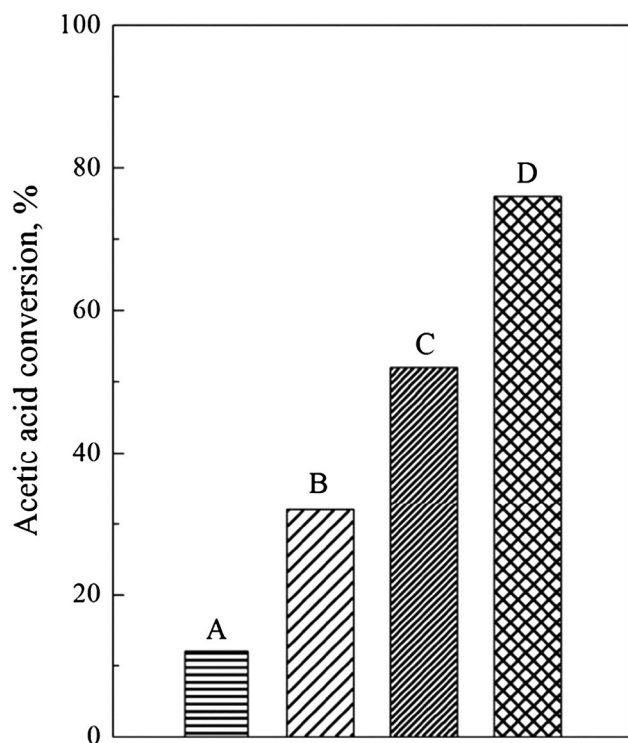

Fig. 6 Effect of different catalyst on the of acetic acid conversion: **a** non-catalyzed reaction; **b** $[H–Pyr]^+[NO_3]^-$; **c** $[H–Pyr]^+[H_2PO_4]^-$; **d** $[H–Pyr]^+[HSO_4]^-$. T = 80 °C; t = 2 h; N_B/N_A = 3/1; C_{cat} 0.0700 mol/L

Taking into account that the cation ($[H–Pyr]^+$) in all samples does not differ (Fig. 2), it becomes clear that the acetic acid conversion depends strongly on the anion nature. At first sight, it seems that the highest acidity (the largest number of protons) possesses $[H–Pyr]^+[H_2PO_4]^-$ sample, and the lowest acidity—$[H–Pyr]^+[NO_3]^-$ one. Consequently, the acetic acid conversion should reach (*i*) a maximum value when esterification process is carried out in the presence of $[H–Pyr]^+[H_2PO_4]^-$ catalyst and (*ii*) the lowest value when $[H–Pyr]^+[NO_3]^-$ is used. However, a maximum X_A value of 76% was obtained when $[H–Pyr]^+[HSO_4]^-$ is used as catalyst, whereas $[H–Pyr]^+[H_2PO_4]^-$ sample gaves conversion of 52% (Fig. 6). In addition, the presence of $[H–Pyr]^+[NO_3]^-$ catalyst increased the acetic acid conversion with 20%, from 12 (non-catalyzed reaction) to 32%. In order to explain the observed absence of correlation between experimental data and proposed catalytic activity of $[H–Pyr]^+[HSO_4]^-$ and $[H–Pyr]^+[H_2PO_4]^-$ samples, the electronic effects in anions $[HSO_4]^-$ and $[H_2PO_4]^-$ were discussed.

Figure 7 shows that the structure of hydrogen sulphate anion ($[(HO)SO_3]^-$) contains three oxygen atoms, which are not attached to hydrogen atoms (in the form of HO^- group). Since the oxygen atom possesses the second highest electronegativity of any atom (3.44 according to Pauling scale) [33], the electron density is drawn toward those atoms by an inductive effect. The inductive effect produced by the three oxygen atoms causes electron density on the sulphur atom to decrease and as a result a slight positive charge ($S^{δ+}$) is formed. The latter is partially compensated by shifting of electron density from the O–H bond. The electron density shift OH → S → O makes the O–H bond more polar and more suitable for cleavage to proton (H^+). Unlike $[(HO)SO_3]^-$, dihydrogen phosphate anion ($[(HO)_2PO_2]^-$) possesses two oxygen atoms, unbounded to hydrogen atoms (Fig. 7). It would mean that polarization of OH groups in $[(HO)_2PO_2]^-$ would be less pronounced than that in $(HO)SO_3]^-$.

Based on the observed electronic effects in anions $[HSO_4]^-$ and $[H_2PO_4]^-$, it could be concluded that $[H–Pyr]^+[HSO_4]^-$ sample may generate a greater
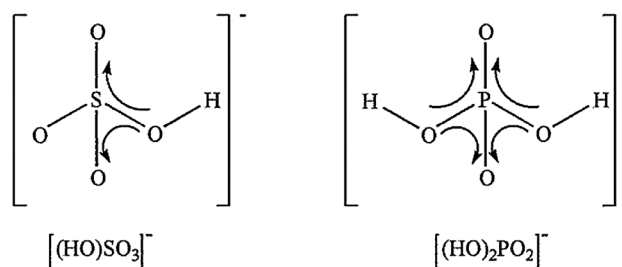

Fig. 7 Structure of anions $[HSO_4]^-$ and $[H_2PO_4]^-$

number of hydrogen cations during the esterification reaction in comparison with $[H–Pyr]^+[H_2PO_4]^-$. In other words, the acetic acid conversion during esterification could increase more rapidly in the presence of $[H–Pyr]^+[HSO_4]^-$ catalyst than of $[H–Pyr]^+[H_2PO_4]^-$. The greater capacity of $[H–Pyr]^+[HSO_4]^-$ to produce protons is confirmed by the K_A values of cation $[H–Pyr]^+$ and anions $[HSO_4]^-$ and $[H_2PO_4]^-$. The dissociation constant value of $[H–Pyr]^+$ is 6.7×10^{-6} ($pK_A = 5.17$), while it values for anions $[HSO_4]^-$ and $[H_2PO_4]^-$ are 1.0×10^{-2} ($pK_A = 2.00$) and 6.2×10^{-8} ($pK_A = 7.21$), respectively [34]. The valued kinetic constant for $[H–Pyr]^+[HSO_4]^-$, $[H–Pyr]^+[H_2PO_4]^-$ and $[H–Pyr]^+[NO_3]^-$ at given reaction conditions were 19.38 ± 2.53 (L/mol.min, $\times 10^{-4}$); 10.12 ± 0.83 (L/mol.min, $\times 10^{-4}$) and 5.28 ± 0.59 (L/mol.min, $\times 10^{-4}$), respectively. Since, $[H–Pyr]^+[HSO_4]^-$ sample possesses a higher catalytic activity than $[H–Pyr]^+[H_2PO_4]^-$ and $[H–Pyr]^+[NO_3]^-$, it was preferred as a catalyst for further studies.

3.4 Effect of Catalyst Concentration

The amount of catalyst plays a major role in the conversion of carboxylic acid to ester (esterification reaction). In a batch process the interaction between acid and catalyst is much more pronounced at the start of the reaction since the concentration of former is high. However, during reaction progress the acid concentration decreases which leads to poorer acid–catalyst interaction. At this point, the amount of catalyst plays a major role in increasing the overall conversion. In this study, the effect of catalyst concentration (C_{cat}) on the conversion value of acetic acid to *n*-butyl acetate was studied with respect to time (Fig. 8). The acetic acid conversion at non-catalytic reaction is also added to the data in Fig. 8.

It was observed that the value of acetic acid conversion during esterification in the absence of catalyst (non-catalyzed reaction) is 12% at 120 min reaction time. The percentage conversion gradually increases as the catalyst loading is increased. When C_{cat} increases from 0.0350 to 0.1050 mol/L, X_A varies from 66 to 78% (at 2 h). Zondervan et al. [35] investigated the esterification of myristic acid with propanol using *p*-toluene sulphonic acid as catalyst and showed that the increasing of catalyst loading enhanced the number of H^+ ions available for acid activation. Thus, higher conversion value (78%) at catalyst concentration of 0.1050 mol/L, with respect to the conversion value (66%) at $C_{cat} = 0.0350$ mol/L was related to a greater number of formed active carbonyl complexes. The rate constant values of 2.12 ± 0.14 (L/mol.min, $\times 10^{-4}$); 13.18 ± 0.98 (L/mol.min, $\times 10^{-4}$); 19.38 ± 2.53 (L/mol.min, $\times 10^{-4}$) and 47.31 ± 3.11 (L/mol.min $\times 10^{-4}$) were
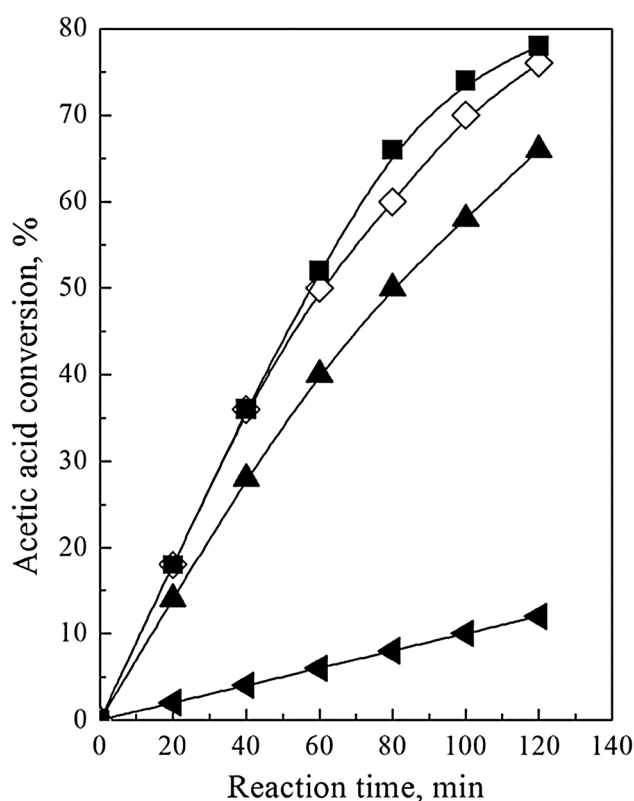

Fig. 8 Effect of catalyst concentration on the acetic acid conversion. C_{cat}: *filled left pointing triangle* 0.0000 mol/L (non-catalytic reaction); *Filled triangle* 0.0350 mol/L; *diamond* 0.0700 mol/L and *filled squared* 0.1050 mol/L. T = 80 °C; $N_B/N_A = 3/1$

obtained for the blank (non-catalyzed) reaction and the esterification carried out using 5, 10 and 15 wt% $[H–Pyr]^+[HSO_4]^-$ catalyst, respectively.

The observed alteration in acetic acid conversion can be confirmed by calculating the rate of reaction as a function of different catalyst loading. In terms of acetic acid conversion [Eq. (1)], the kinetic model [Eq. (2)] can be written as:

$$-r_A = -C_{Ao}(dX_A/dt) \tag{4}$$

After rearranging and integration, Eq. (4) becomes as follows:

$$r_A = (C_{A0}X_A)/t \tag{5}$$

Substituting Eq. (1) in Eq. (5):

$$r_A = (C_{A0} - C_A)/t \tag{6}$$

The effect of catalyst loading on the reaction rate is shown in Fig. 9. Results demonstrated that the reaction rate is directly proportional to catalyst concentration, i.e. with increasing of C_{cat}, the esterification rate also increases.
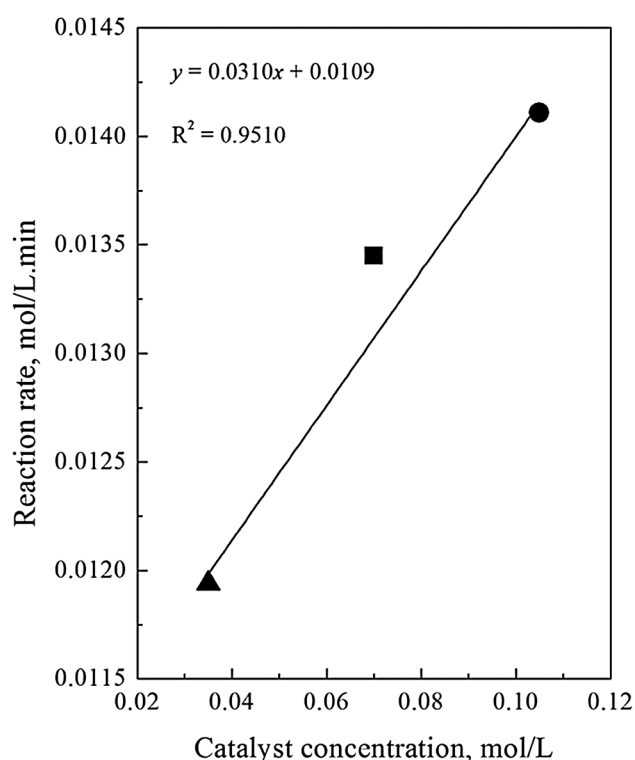
Fig. 9 Effect of catalyst concentration on the reaction rate. C_{cat}: *filled triangle* 0.0350 mol/L; *filled squared* 0.0700 mol/L; *filled circle* 0.1050 mol/L. T = 80°C; N_B/N_A = 3/1; t = 2 h

Fig. 10 Effect of molar ratio of *n*-butanol-to-acetic acid on the of acetic acid conversion. N_B/N_A: *filled left pointing triangle* 1/1; *filled circle* 3/1; *diamond* 5/1; *filled squared* 7/1. T = 80°C; C_{cat} = 0.0700 mol/L; t = 2 h

3.5 Effect of Molar Ratio

The alteration of acetic acid conversion as a function of molar ratio of *n*-butanol-to-acetic acid (N_B/N_A = 1/1–7/1) was established at temperature of 80 °C, catalyst concentration 0.0700 mol/L and reaction time 2 h (Fig. 10).

Experimental data indicated that N_B/N_A value significantly affects the acetic acid conversion to *n*-butyl acetate. The variation of molar ratio value from 1/1 to 3/1 slightly increased the conversion of acetic acid from 72 to 76% (Fig. 10). It was evident that with increasing of N_B/N_A up to 5/1, the acetic acid conversion notably enhances and reaches a value of 96%. At a molar ratio of 7/1, the highest acid conversion (98%) was observed.

Figure 10 clearly presents that the conversion of acetic acid decreases by reduction of the molar ratio value. In other words, when the initial concentration of *n*-butanol in reactor decreases (molar ratio becomes lower), acetic acid conversion diminishes. This observation was not surprising, considering the fact that low concentration of reactants shifts the reaction equilibrium toward the right side of stoichiometry equation [36, 37]. It was mentioned above that the acetic acid conversion at molar ratio of 5/1 and 7/1 is 96 and 98%, respectively. Therefore, it can be concluded that the ratio of alcohol-to-acid required to attain a maximum
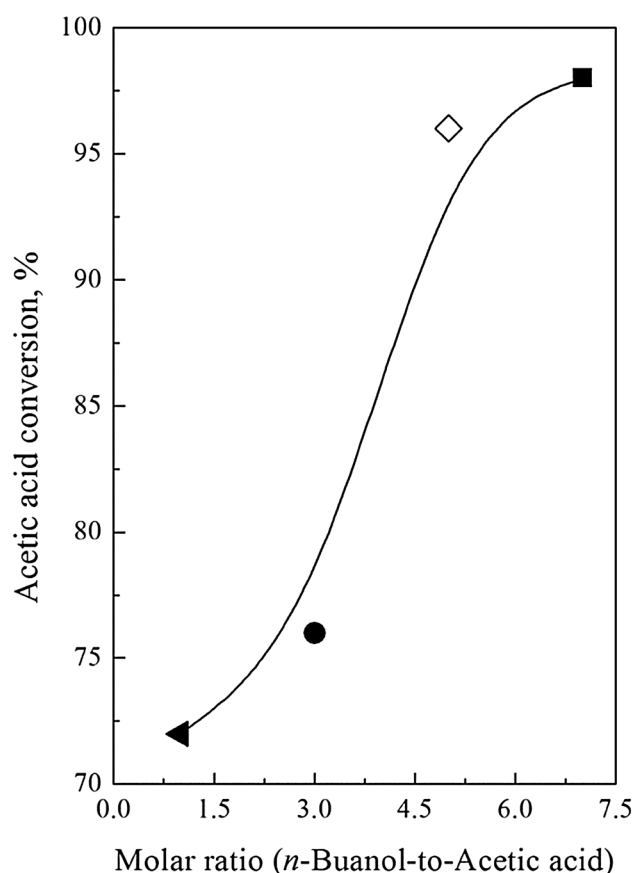
of acetic acid conversion at given reaction conditions is in range from 5/1 to 7/1. The results showed that the kinetic constant value depends highly on the reactants molar ratio. Accordingly, for N_B/N_A = 1/1, 3/1, 5/1 and 7/1 the kinetic constant values of 14.16 ± 0.83 (L/mol.min, $\times 10^{-4}$); 19.38 ± 2.53 (L/mol.min, $\times 10^{-4}$); 34.28 ± 5.41 (L/mol.min, $\times 10^{-4}$) and 27.08 ± 2.73 (L/mol.min, $\times 10^{-4}$) were obtained, respectively.

3.6 Effect of Reactant Concentration

The reaction rate (calculated from Eq. 5) was determined by varying the concentration of reactants (acetic acid, C_A, and *n*-butanol, C_B). The results of these variations are shown in Fig. 11a, b.

Figure 11a represents the existence of a positive linearly relationship ($R^2 = 0.9939$) between the reaction rate and concentration of acetic acid. It was found that the increasing of acetic acid concentration from 1.2057 to 3.5661 mol/L resulted in increment of reaction rate from 0.0098 to 0.0214 mol/L.min. A possible explanation of
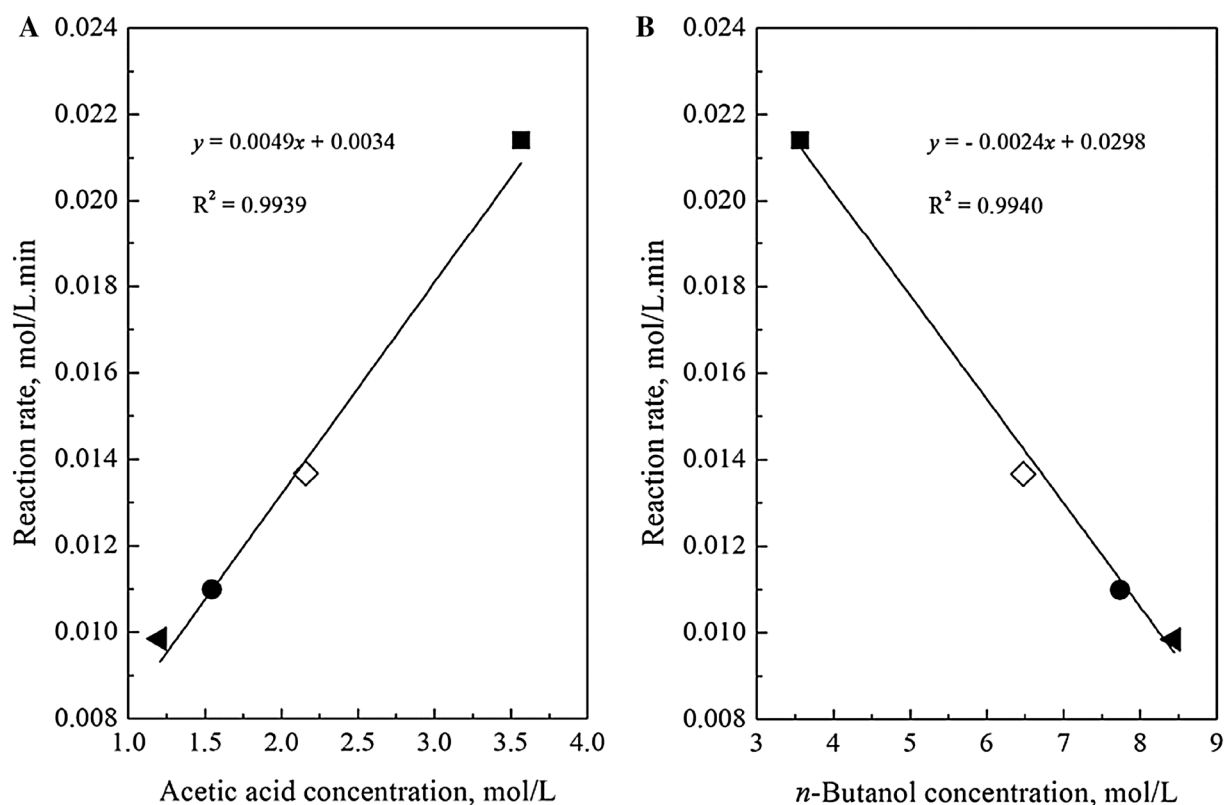
Fig. 11 Effect of acetic acid and *n*-butanol concentration on the reaction rate. **a** *Filled left pointing triangle* 1.2057 mol/L; *Filled circle* 1.5476 mol/L; *diamond* 2.1585 mol/L; *Filled squared* 3.5661 mol/L.

b *Filled left pointing triangle* 8.4401 mol/L; *Filled circle* 7.7382 mol/L; *diamond* 6.4755 mol/L; *Filled squared* 3.5661 mol/L. T = 80°C; C_{cat} = 0.0700 mol/L; t = 2 h

the observed tendency could be the high concentration of acetic acid, which favors the forward reaction [35]. In other words, the high concentration of acetic acid shifts the chemical equilibrium to reaction products. During the esterification progress the concentration of acetic acid diminishes and hence the reaction rate decreases.

In contrast to the effect of acetic acid concentration, the increasing of *n*-butanol concentration from 3.5661 to 8.4401 mol/L caused the rate of esterification to decrease linearly (R^2 = 0.9940) from 0.0214 to 0.0098 mol/L (Fig. 11b). This phenomenon suggests that a certain (critical) value of acetic acid concentration was achieved. It has been already mentioned that the maximum conversion of acetic acid (96–98%) was obtained when molar ratio varies from 5/1 to 7/1 (see pt. 3.5). At those values of N_B/N_A, the acetic acid concentration was changed from 1.5476 to 1.2057 mol/L. Above a critical value of *n*-butanol concentration (in the current paper it varies from 7.7381 to 8.4401 mol/L at N_B/N_A = 5/1–7/1), a decreasing in overall acetic acid conversion due to a dilution effect was observed. The latter reduces the rate of esterification process, according to Eq. 5.

3.7 Effect of Reaction Temperature

The effluence of reaction temperature on the acetic acid conversion and reaction rate was established at 80 and 100°C using inert solvents, hexane and heptane, respectively (Fig. 12a, b).

The experimental data in Fig. 12a showed that the effect of reaction temperature on both the conversion of acetic acid and rate of esterification is significant. For example, at temperature of 80°C the conversion of acetic acid was 76% and it increases up to 98% when the reaction temperature goes up to 100 °C. The latter was due to a greater number of effective impacts between reactants, a consequence of the acquired kinetic energy. The observed alteration in acetic acid conversion (from 76 to 98%) indicates that at reaction temperature of 100 °C the acetic acid concentration should decrease more rapidly, compared to the decreasing of acetic acid concentration at 80 °C. The latter means that at temperature of 100°C the reaction rate decreases faster than the rate at 80 °C, according to Eq. 5. Calculations showed that the rate of esterification at temperature of 100 °C deceases with 46% (from 0.0344 to 0.0185 mol/L.
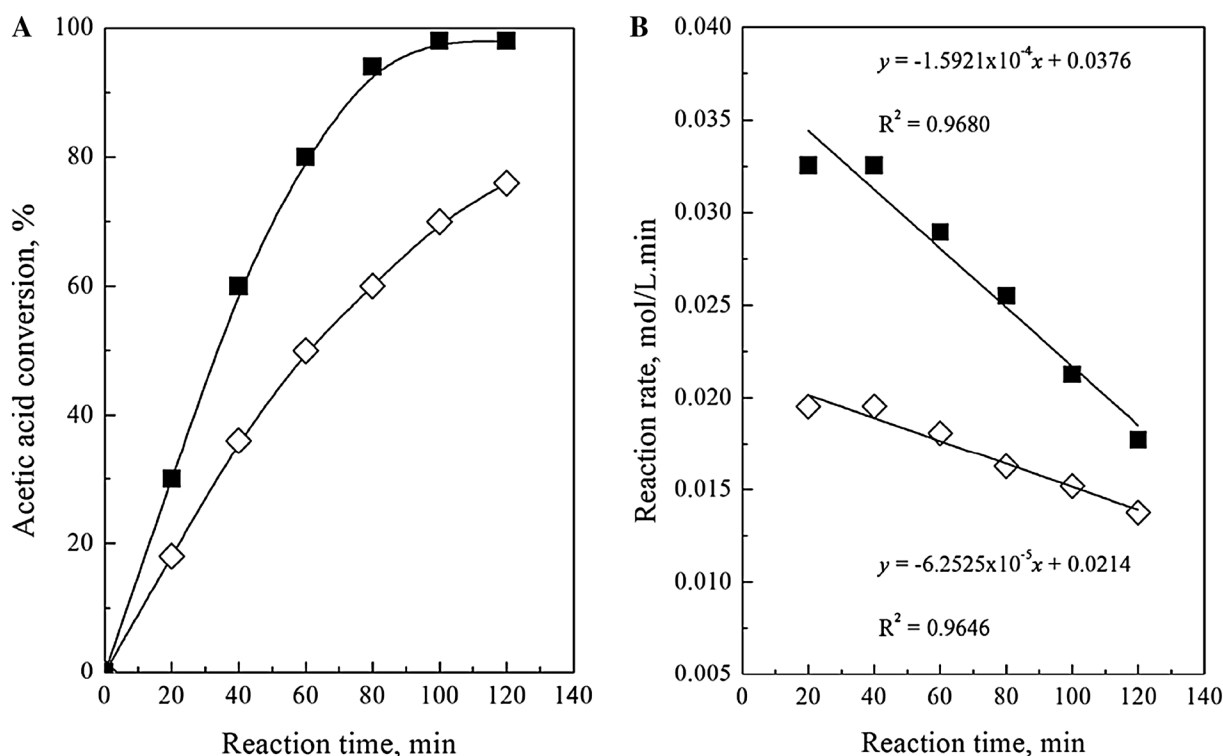
Fig. 12 Effect of temperature on the acetic acid conversion and reaction rate. *diamond* 80°C; *Filled squared* 100°C. C_{cat} = 0.0700 mol/L; N_B/N_A = 3/1

min), while at temperature of 80 °C—with 31% (from 0.0201 to 0.0139 mol/L.min) (Fig. 12b). The kinetic constant value at reaction temperature of 100, 80 and 60 °C was 31.43 ± 5.64 (L/mol.min, $\times 10^{-4}$); 19.38 ± 2.53 (L/mol. min, $\times 10^{-4}$) and 7.27 ± 0.65 (L/mol.min, $\times 10^{-4}$), respectively. Based on the Arrhenius law, values of 77.25 kJ/mol and 767.39 kmol/min $\times 10^4$ were obtained as activation energy and pre-exponential factor, respectively.

4 Conclusions

Three acidic ionic liquids: [H–Pyr]$^+$[HSO$_4$]$^-$, [H–Pyr]$^+$[H$_2$PO$_4$]$^-$ and [H–Pyr]$^+$[NO$_3$]$^-$ were synthesized and tested as catalysts for direct esterification of acetic acid with *n*-butanol to produce *n*-butyl acetate. It was found that the obtained ionic liquids are thermally stable up to 140 °C. Above that temperature they undergo thermal decomposition. Therefore their use as catalysts for esterification requires reaction temperatures lower than 140 °C. The catalytic activity was established to depend on the ionic liquid structure. Maximum conversion of acetic acid (76%) is provided when [H–Pyr]$^+$[HSO$_4$]$^-$ was used as catalyst, followed by [H–Pyr]$^+$[H$_2$PO$_4$]$^-$ (52%) and [H–Pyr]$^+$[NO$_3$]$^-$ (32%). The observed catalytic behavior was attributed to different Brønsted acidity of the anion.

The acetic acid conversion increased proportionally to catalyst concentration due to a greater number of formed active carbonyl complexes. It was established that the molar ratio of alcohol-to-acid required to attain a maximum of acetic acid conversion is in range from 5/1 to 7/1. While the increase of acetic acid concentration enhanced esterification reaction rate, the augmentation of *n*-butanol concentration diminished it. It was proposed that critical values of acetic acid and *n*-butanol concentration are achieved. Above a critical value of *n*-butanol concentration a decreasing in overall acetic acid conversion due to a dilution effect was observed. The acetic acid conversion increased with an increasing in temperature, which confirmed that the reaction is kinetically controlled.

References

1. Steinigeweg S, Gmehling J (2002) Ind Eng Chem Res 41:5483
2. Ronnback R, Salmi T, Vuori A, Haario H, Lehtonen J, Sundqvist A, Tirronen E (1997) Chem Eng Sci 52:3369
3. Peng X, Wang L (2015) Chem Eng Technol 38:223
4. Tao D-J, Wu Y-T, Zhou Z, Geng J, Hu X-B, Zhang Z-B (2011) Ind Eng Chem Res 50:1989
5. Sawant DP, Vinu A, Justus J, Srinivasu P, Halligudi SB (2007) J Mol Catal A 276:150
6. Das J, Parida KM (2007) J Mol Catal A 264:248
7. Jermy BR, Pandurangan A (2005) J Mol Catal A 237:146

8. Gangadwala J, Mankar S, Mahajani S, Kienle A, Stein E (2003) Ind Eng Chem Res 42:2146
9. JagadeeshBabu PE, Sandesh K, Saidutta MB (2011) Ind Eng Chem Res 50:7155
10. Mitran G, Pavel OD, Marcu IC (2013) J Mol Catal A 370:104
11. Mitran G, Yuzhakova T, Popescu I, Marcu I-C (2015) J Mol Catal A 396:275
12. Fraga-Dubreuil J, Bourahla K, Rahmouni M, Bazureau JP, Hamelin J (2002) Catal Commun 3:185
13. Tao D-J, Lu X-M, Lu J-F, Huang K, Zhou Z, Wu Y-T (2011) Chem Eng J 171:1333
14. Duan Z, Gu Y, Zhang J, Zhu L, Deng Y (2006) J Mol Catal A 250:163
15. Zhao D, Liu M, Zhang J, Li J, Ren P (2013) Chem Eng J 221:99
16. Zhou B, Fang Y, Gu H, Zhang S, Huang B, Zhang K (2009) Chem Eng China 3:211
17. Yang J, Zhou L, Guo X, Li L, Zhang P, Hong R, Qiu T (2015) Chem Eng J 280:147
18. Ganeshpure PA, George G, Das J (2008) J Mol Catal A 279:182
19. Zhao YW, Long JX, Deng FG, Liu XF, Li Z, Xia CG, Peng JJ (2009) Catal Commun 10:732
20. Boopalachandran P, Sheu H-L, Laane J (2012) J Mol Struct 1023:61
21. Matuszek K, Chrobok A, Coleman F, Seddon KR, Swadźba-Kwaśny M (2014) Green Chem 16:3463
22. Moosavi-Zare AR, Zolfigol MA, Zarei M, Zare A, Khakyzadeh V (2013) J Mol Liq 186:63
23. Khaligh NG, Ghasem-Abadi PG (2014) Chin J Catal 35:1126
24. Shirini F, Khaligh NG (2013) J Mol Liq 177:386
25. Chtioui A, Jouini A (2004) J Chem Cryst 34:43
26. Joe IH, Jayakumar VS, Aruldhas G (1995) J Solid State Chem 120:343
27. Batsanov AS (2004) Acta Cryst E 60:2426
28. Goebbert DJ, Garand E, Wende T, Bergmann R, Meijer G, Asmis KR, Neumark DM (2009) J Phys Chem A 113:7584
29. Liu Y, Lotero E, Goodwin JG Jr (2006) J Catal 242:278
30. Salciccioli M, Stamatakis M, Caratzoulas S, Vlachos DG (2011) Chem Eng Sci 66:4319
31. Schmitt M, Blagov S, Hasse H (2008) Ind Eng Chem Res 47:6014
32. Zhang HL, Feng GY, Wei TJ (1995) Henan Chem Ind 2:5
33. Pauling L (1932) JACS 54:3570
34. Sarmini K, Kenndler E (1999) J Biochem Biophys Methods 38:123
35. de Jong MC, Feijt R, Zondervan E, Nijhuis TA, de Haan AB (2009) Appl Catal A 365:141
36. Altıokka MR, Ödeş E (2009) Appl Catal A 362:115
37. Yamakawa T, Tsai PK, Shinoda S (1992) Appl Catal A 92:L1